



Bifurcations analysis in implicit maps through the dynamics of cumulated surface errors in milling

Adam K. Kiss · Daniel Bachrathy

Received: 25 February 2021 / Accepted: 24 April 2022
© The Author(s) 2022

Abstract In this contribution, we examine the evolution of surface errors during consecutive milling operations. Its description is based on a nonlinear implicit map, which is suitable to investigate the surface quality. It describes the series of consecutive Surface Location Errors (SLE) in roughing operations. As one of the principal results of the paper, bifurcations related to the fixed point of the implicit map are analyzed via normal form theorem. We determined a formula for the criticality of the bifurcation, which allows the approximate computation of the arising period-two solution. The method is demonstrated for the surface error model of milling, and the results are verified by numerical computations. Although the amplitude of the SLE would be negligible, its derivatives has a great influence in the model, which can cause stability problems.

Keywords Milling · Stability · Surface location error · Implicit map · Bifurcation analysis

1 Introduction

In the production industry, milling is a widely used manufacturing method. Due to the intermittent nature

of the material removal processes, the cutting edges enter and exit into the material periodically. This phenomenon leads to two kinds of vibration, which may limit the achievable productivity. The mitigation of these vibrations is still an open research field [1]. One of them is referred to as chatter, which is a self-excited oscillation relating to the stability loss of the cutting process [2] while the other one is related to large amplitude forced vibration near to resonant spindle speeds [3].

The most accepted phenomenon to describe chatter is the so-called surface regeneration effect or memory effect [4,5], that is the instantaneous chip thickness depends on the present and the delayed relative positions between the cutting tool and the workpiece. It can be modeled by delay-differential equations (DDE) [6], for which the stability limit draws the line between chatter-free (stable) and chatter (unstable) vibrations in the space of the technological parameters. That is referred to as stability chart or stability lobe diagram illustrating chatter-free regions [7]. These charts can be used to optimize roughing operations, where the workpiece oversize is removed with several consecutive immersions. Usually, the most productive chatter-free parameter regions, where the highest material removal can be achieved, are located near the resonant spindle speeds. However, large amplitude vibrations occur there due to the resonant excitation of the periodic milling force [8,9].

This vibration is copied to the surface and creates the so-called surface location error (SLE), which is an off-

A. K. Kiss (✉) · D. Bachrathy
MTA-BME Lendület Machine Tool Vibration Research Group, Department of Applied Mechanics, Faculty of Mechanical Engineering, Budapest University of Technology and Economics, Budapest 1111, Hungary
e-mail: kiss_a@mm.bme.hu

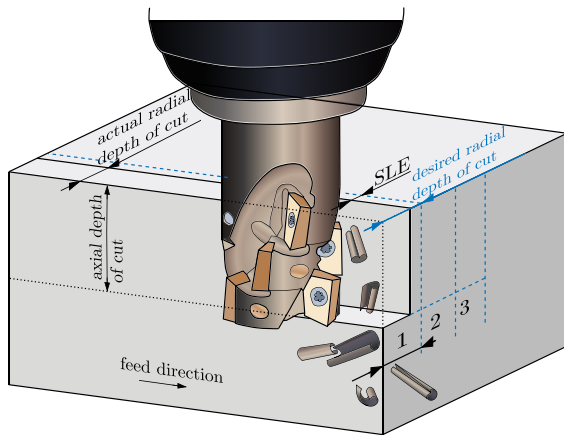


Fig. 1 Effects of the surface error on the radial depth of cut

set error defined by the largest deviation between the machined and the desired surface [10–13]. This SLE directly reduces the radial depth of cut which modifies the machining process (see Fig. 1). Due to the fact that SLE is relevant at finishing operations [10], during the prediction of this surface error, the widely used methods do not consider that the SLE can influence the radial depth of cut. However, in the case study in [14], the measured vibrations amplitude resulting surface errors were in the range of the radial depth of cut. Therefore, the SLE can still have a significant impact on the surface quality in case of consecutive immersions during roughing. At every immersion, the machined surface differs from the desired one due to the SLE. The offset errors modify the radial depth of cut and generate different cutting force, which leads to a modified subsequent surface error. During this process, the SLE can accumulate and the phenomenon leads to a new surface quality parameter denoted by the cumulative surface location error (CSLE).

The general concept of the CSLE was firstly introduced in [15]. In this model, it is considered that the initial surface position is shifted relative to the desired one by the surface location error generated in the previous cut. This leads to an explicit nonlinear scalar map which determines how one SLE develops into another immersion-by-immersions. It is published first in [16], then further investigation relating to measurement-based model was carried out in [17], while experimental validation of this explicit model can be found in [18].

This explicit model is not enough to describe this complex phenomenon, and it has a significant draw-

back, that it considers only the previous SLE error. However, the actual SLE influences the results similarly that leads to completely different results and a much more complex mathematical model. This improved model, where the surface error arises not only from the error in the previous cutting but also from the current one, was first introduced in [19] for turning operation. Here, static deformation error and its evolution were investigated by means of a numerical method, where the corresponding model is based on an implicit nonlinear map. This implicit model describes a similar memory effect that can be found in the general surface regeneration phenomenon [5], and it better describes the process of SLE evolution, since it takes into account not only the events of the past but also the effects of the current error.

In the existing literature for explicit maps, the linear stability analysis and nonlinear investigation [20] such as bifurcation analysis [21] and normal form calculations [22] are extensively investigated while engineering applications are diverse [23–25]. A comprehensive literature review about investigation of explicit maps can be found in [26,27] and all the references therein.

Implicit maps are more complex mathematically. On the one hand, they usually used during discretization in numerical simulation of differential equations, such as the implicit Euler, the implicit Runge–Kutta and the Adams–Moulton methods [28], where the main aspect of the investigations is about the performance and convergence of the numerical solver. On the other hand, implicit maps also occur in engineering applications [29,30]. Linear stability analysis of fixed point can be found in [29,31], while the readers can find more information about implicit systems in [31]. Yet, these works have not addressed normal form calculations in implicit systems and the nonlinear analysis in implicit maps is not discussed. To the best knowledge of the authors, so far the normal form analysis has not been extended to implicit maps.

This paper intends to fill this gap and tackle the challenges arising from the combination of implicit scalar systems and bifurcation analysis. Our contributions are twofold. One of the main goals of this research is to extend the implicit model of the CSLE for milling operation, while the other goal is to understand how these errors are evolving. Therefore, we derive the computational steps of a complete bifurcation analysis with linear and nonlinear investigation of the implicit map.

The rest of the paper is organized as follows. In Sect. 2, we determine the stability of the system by analyzing the fixed point of the corresponding implicit map and calculating its critical normal form coefficients. Via these coefficients, we use analytical formulae to obtain the approximate amplitude of the bifurcating solutions as a function of the bifurcation parameter. Sections 2.1 and 2.2 present the general form of the governing implicit scalar map and the corresponding linear stability analysis of the fixed point. Section 2.3 provides the bifurcation investigation, where the coefficients of the normal forms are given. Then, in Sect. 3, the computation of the SLE and the corresponding mechanical model are briefly discussed. In Sect. 4, the implicit mapping of the SLE values is introduced for consecutive roughing operations and the CSLE is defined. In Sects. 4.1 and 4.2, the linear and nonlinear stability investigation are performed parametrically for SLE mapping based on the results presented in Sect. 2. In Sect. 5, a case study for a selected milling operation is conducted providing the resulting stability charts and bifurcation diagrams. Finally, in Sect. 6, we conclude our findings and discuss future directions.

2 Implicit discrete system

2.1 Governing equation

Consider the following governing nonlinear implicit scalar discrete map depending on a parameter in the form

$$x_{i+1} = f(x_i, x_{i+1}; \alpha), \tag{1}$$

where $x \in \mathbb{R}$ and $\alpha \in \mathbb{R}$ represent state variable and bifurcation parameter, respectively, and $f : \mathbb{R} \times \mathbb{R} \times \mathbb{R} \rightarrow \mathbb{R}$ is supposed to be sufficiently smooth (differentiable). Note that this system is implicit, since the state variable appears at the left and right hand side in (1).

Here we use the following implicit equation notion for (1)

$$F(x_i, x_{i+1}; \alpha) = f(x_i, x_{i+1}; \alpha) - x_{i+1} = 0, \tag{2}$$

where F has the same properties as f .

According to the Implicit Function Theorem, if $\frac{\partial F}{\partial x_i}$ is nonsingular, then exists a smooth locally defined function

$$x_{i+1} = g(x_i), \tag{3}$$

where $g : \mathbb{R} \rightarrow \mathbb{R}$ and it satisfies that $F(x_i, g(x_i); \alpha) = 0$. Here the degree of smoothness of the function g is the same as that of F and generally g cannot be expressed explicitly in closed form.

2.2 Fixed point and its linear stability

Iterating the map (1), the solution may converge to a fixed point, where the state maps to itself, that is $x_i = x_{i+1} =: x^*$, which indeed satisfies

$$F(x^*, x^*; \alpha) = 0. \tag{4}$$

Note that as a consequence of the Implicit Function Theorem, the fixed point also satisfies $x^* = g(x^*)$.

We are interested in to analyze the local dynamics in the vicinity of the fixed point. First, expanding (3) into Taylor series and eliminating the higher-order terms and by introducing the perturbation $u_i = x_i - x^*$, the implicit variational map can be defined as

$$u_{i+1} = g'(x^*)u_i + \mathcal{O}(u_i^2). \tag{5}$$

Note that $u \equiv 0$ is the trivial solution of (5), and the bifurcation analysis of x is equivalent to the analysis of the trivial solution $u \equiv 0$. In (5), $g'(x)$ is derived by the total differentiation of (2) after substituting (3) and dropping the notation of the parameter dependence:

$$\begin{aligned} & \left. \frac{d}{dx_i} F(x_i, g(x_i)) \right|_{x^*} \\ &= \left. \frac{\partial F}{\partial x_i} \right|_{x^*} + \left. \frac{\partial F}{\partial g(x_i)} \right|_{x^*} g'(x^*) = 0. \end{aligned} \tag{6}$$

It is referred to as implicit function derivation theorem in the Appendix of [29]. This form can also be found in [31] after Eq. (4.11). By using (3), one can find identity $\frac{\partial F}{\partial g(x_i)} = \frac{\partial f}{\partial x_{i+1}}$, and using (2) the partial derivatives simplify to $\frac{\partial F}{\partial x_i} = \frac{\partial f}{\partial x_i}$ and $\frac{\partial F}{\partial x_{i+1}} = \frac{\partial f}{\partial x_{i+1}} - 1$. The coefficient of the linear term in (5) can be rearranged as

$$g'(x^*) = - \left. \frac{\frac{\partial f}{\partial x_i}}{\frac{\partial f}{\partial x_{i+1}} - 1} \right|_{x^*}, \tag{7}$$

For convenient description, we will use a short notation $f_a := \frac{\partial f}{\partial x_i}$ and $f_b := \frac{\partial f}{\partial x_{i+1}}$ for the partial derivatives with respect to the state variables in the first and second argument of f . Then the characteristic equation of (5) becomes

$$\mu + \left. \frac{f_a}{f_b - 1} \right|_{x^*} = 0, \tag{8}$$

where the characteristic multiplier is

$$\mu = - \left. \frac{f_a}{f_b - 1} \right|_{x^*}. \tag{9}$$

If $|\mu| < 1$, then the fixed point is linearly asymptotically stable, otherwise it is unstable [26,27]. By investigating (8), one can show that the system loses stability via flip (period doubling) bifurcation at a critical parameter α_{cr} where $\mu = -1$ which leads to period-2 solutions around the fixed point and via fold (saddle-node) bifurcation at a critical parameter α_{cr} where $\mu = 1$. Note that only flip and fold bifurcations are possible since (1) is a scalar map. Note that for the so-called Neimark–Sacker (torus) bifurcation, one needs at least two-dimensional system in (1) [26]; however, it is out of the scope of the current work since, in our application, the SLE is scalar-valued.

2.3 Bifurcation analysis

The linear stability analysis only provides information about the local behavior around the fixed point, but does not give information about how the system behaves farther from it. Furthermore, it does not provide information on how close to the fixed point the local stability behavior is valid.

In this section, we perform the bifurcation analysis of the implicit system in (1) which can approximate the domain of attraction providing insight into the global behavior of the system. Based on the theory of nonlinear dynamical systems, the dominant dynamics can be investigated on an invariant manifold. In case of scalar system, this manifold is described equivalently by the map in (3). Setting the system parameter α close to the critical bifurcation parameter α_{cr} , one can approximate the essential dynamics by the normal form equations on the manifold. For the normal form calculation and bifurcation analysis, the third-order approximation of the map (3) is needed [26]

$$u_{i+1} = g'(x^*)u_i + \frac{1}{2}g''(x^*)u_i^2 + \frac{1}{6}g'''(x^*)u_i^3 + \mathcal{O}(u_i^4). \tag{10}$$

In this way, arising solutions and their stability can be characterized where the fixed point undergoes a bifurcation.

Since the governing equation is implicit in the state variable, the derivation of its third-order approximation

is based on the total differentiation (implicit differentiation) of (2). The derivation steps are similar as presented in Sect. 2.2, but higher-order total derivatives are needed. The detailed derivation of the third-order approximation is discussed in Appendix A.

2.3.1 Flip bifurcation

Using the nonlinear near-identity transform in [26,32,33] $u_i = \hat{u}_i + \frac{g''(x^*)}{4}\hat{u}_i^2$ for flip-type bifurcation $\mu = -1$, the second-order term can be eliminated yielding the normal form

$$\hat{u}_{i+1} = -\hat{u}_i - \delta_{cr}\hat{u}_i^3, \tag{11}$$

where the leading coefficient reads as (see the formulae after Eq. (5.69) in [26])

$$\delta_{cr} = -\left(\frac{1}{4}(g''(x^*))^2 + \frac{1}{6}g'''(x^*)\right), \tag{12}$$

where the complete formula for the derivatives of g can be found in Appendix A.

In case of flip bifurcation, in the vicinity of the bifurcation point α_{cr} the steady-state oscillations can be approximated as a function of the bifurcation parameter α [26] as

$$\hat{u}_i = \sqrt{\frac{\gamma_{cr}}{\delta_{cr}}(\alpha - \alpha_{cr})}(-1)^i, \tag{13}$$

where γ_{cr} and δ_{cr} are the so-called root tendency and leading coefficient, respectively. By taking the derivative of the characteristic equation (8) at the critical point α_{cr} , one can obtain the root tendency

$$\gamma_{cr} = \left. \frac{d\mu}{d\alpha} \right|_{x^*, \alpha_{cr}} = \left. \frac{f_{b;\alpha} - f_{a;\alpha}}{f_a} \right|_{x^*, \alpha_{cr}}, \tag{14}$$

where $f_{a;\alpha} := \frac{\partial^2 f}{\partial x_i \partial \alpha}$ and $f_{b;\alpha} := \frac{\partial^2 f}{\partial x_{i+1} \partial \alpha}$ denote the mixed partial derivatives with respect to the state variables and the bifurcation parameter. This root-tendency represents the speed by which the critical characteristic multiplier crosses the -1 during the flip bifurcation leading to stability loss.

Based on the above derivation, we can define the closed-form formula for the leading coefficient in case of implicit scalar system:

$$\delta_{cr} = - \frac{3(f_{aa} - f_{bb})(f_{aa} - 2f_{ab} + f_{bb})}{12f_a^2} + \frac{2f_a(f_{aaa} - 3f_{aab} + 3f_{abb} - f_{bbb})}{12f_a^2} \Big|_{x^*, \alpha_{cr}}, \tag{15}$$

where the second- and third-order partial derivatives of f with respect to the state variables are defined based on the indices, e.q.: $f_{ab} := \frac{\partial^2 f}{\partial x_i \partial x_{i+1}}$ and $f_{aab} := \frac{\partial^3 f}{\partial x_i^2 \partial x_{i+1}}$.

The general conditions for the existence and uniqueness of the arising oscillations are provided by means of the transversality condition $\gamma_{cr} \neq 0$ and the nondegeneracy condition $\delta_{cr} \neq 0$, [26]. Here, we assume that these conditions are fulfilled.

The criticality of the flip bifurcation is determined by the sign of the leading coefficient in (15). The bifurcation is subcritical and the arising oscillations in (13) are unstable for $\delta_{cr} > 0$ while the bifurcation is supercritical and the oscillations are stable for $\delta_{cr} < 0$. Note that the arising oscillation of the state variable can be approximated as $x_i = x^* + u_i$.

2.3.2 Fold bifurcation

In case of fold bifurcation, the critical characteristic multiplier is $\mu_{cr} = 1$ and the corresponding normal form reads as

$$u_{i+1} = u_i + \frac{1}{2}g''(x^*)u_i^2, \tag{16}$$

which can be obtained by the second-order approximation of map (3). Here, the genericity conditions for the existence and uniqueness are provided by the nondegeneracy condition $g''(x^*) \neq 0$ and the transversality condition $\left. \frac{\partial g}{\partial \alpha} \right|_{s^*} \neq 0$ [26].

In the followings, the evaluation of the series of the surface location error (SLE) values in milling operations and the corresponding implicit map is investigated to demonstrate the above derivations.

3 Computation of surface location error

In this section, the mechanical model of the milling process and the main steps of the SLE computation are summarized based on [14]. Here, the mechanical model is kept as simple as it is possible but detailed enough to contain all relevant dynamics for the SLE computation. Therefore, the quality of the machined surface property is determined numerically in case of straight fluted tool. The workpiece is considered as a rigid body, and the milling tool is described as a flexible part (presented in Fig. 2). In case of chatter-free machining process, the forced stationary periodic motion can be calculated as the solution of the following ordinary differential

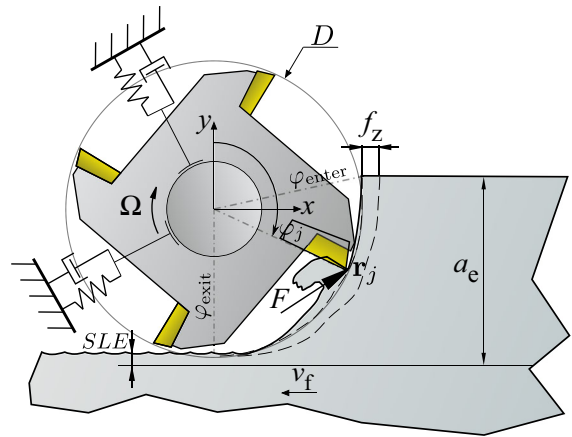


Fig. 2 The mechanical model of the milling process and representation of the surface location error in case of down-milling operation

equation (ODE) in the modal space by using the modal coordinates vector of $\mathbf{q}(t) \in \mathbb{R}^d$

$$\ddot{\mathbf{q}}(t) + [2\zeta_k \omega_{n,k}] \dot{\mathbf{q}}(t) + [\omega_{n,k}^2] \mathbf{q}(t) = \mathbf{U}^T \mathbf{F}(t), \tag{17}$$

where \mathbf{F} is the periodic directional force acting on the workpiece, d is the number of degrees of freedom, and the modal parameters such as ζ_k , $\omega_{n,k}$ and \mathbf{U} are the natural angular frequency, the corresponding relative damping ratio and the modal transformation matrix, respectively [34].

In this study, linear force model is considered [35] in which the resultant cutting force is linearly proportional to the chip width w and the chip thickness h . The chip thickness consists of two parts, stationary and dynamic chip thickness [5]. The stationary one is resulted from the projection of the feed motion in the direction of the cutting edge. The dynamic one corresponds to the surface regenerative effect of the machining process [4]. Now only the periodic motion is analyzed which creates the surface error for which the dynamical components cancel out; hence, only the stationer component of the chip thickness is used. For the SLE computation, only the forced periodic vibration of the tool-tip is needed in the direction of the machined surface normal (perpendicular to the tool path). Therefore in our model, only the dynamics along the y direction are analyzed, and only the y component of the resultant cutting force acting on the tool-tip is included. The radial and the tangential cutting force component projected to the y

direction is given by

$$F_y(t) = \sum_{j=1}^Z a_p f_Z \sin \varphi_j(t) g(\varphi_j(t)) (K_r \cos \varphi_j(t) - K_t \sin \varphi_j(t)), \tag{18}$$

where Z is the number of the cutting edges, a_p is the axial depth of cut, f_Z is the feed per tooth, K_r and K_t are the radial and tangential cutting force coefficients, respectively [14].

These parameters are usually identified by several cutting experiments for given cutting parameters and tool geometry [36]. The current angular position of the j th cutting edge is denoted by $\varphi_j(t) = \Omega t + 2\pi(j - 1)/Z$, where Ω is the angular spindle speed in rad/s. Note that the spindle speed in round-per-minute (rpm) is usually denoted with n in the machining society. The so-called screen function g indicates that the j th edge is in contact with the material between the enter φ_{enter} and exit angle φ_{exit} only

$$g(\varphi) = \begin{cases} 1 & \text{if } \varphi_{\text{enter}} < \varphi < \varphi_{\text{exit}}, \\ 0 & \text{otherwise.} \end{cases} \tag{19}$$

These angles are the nonlinear functions of the dimensionless radial depth of cut $a = a_e/D$, reads as

$$\begin{aligned} \varphi_{\text{enter}} &= \begin{cases} 0 & \text{if up-milling,} \\ \arccos 2a - 1 & \text{if down-milling,} \end{cases} \\ \varphi_{\text{exit}} &= \begin{cases} \arccos 1 - 2a & \text{if up-milling,} \\ \pi & \text{if down-milling,} \end{cases} \end{aligned} \tag{20}$$

where a_e is the radial depth of cut and D is the diameter of the tool.

In order to avoid uncertainties resulting from the modal fitting, frequency response function $H(\omega)$ can be directly used to compute the forced stationary vibration

$$y(t) = \mathcal{F}^{-1}(H(\omega)\phi_y(\omega)), \tag{21}$$

where $\phi_y(\omega)$ denotes the Fourier transformed the cutting force (18) and \mathcal{F}^{-1} denotes the inverse Fourier transformation. The motion of the j th cutting edge is described by means of the superposition of the rotary motion of the edge and the forced stationary vibration of the tool centre point $y(t)$, that is

$$r_{y,j}(t) = y(t) + \frac{D}{2} \cos \varphi_j(t). \tag{22}$$

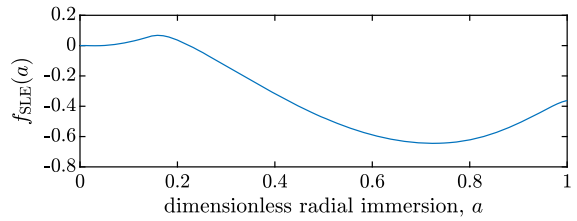


Fig. 3 Resulted dimensionless surface location error in the function of the dimensionless radial depth of cut

Then the SLE is determined as the extremum of the cutting edge motion:

$$\begin{aligned} SLE &= \max_{t,j} (r_{y,j}(t)) - \frac{D}{2} \quad (\text{up-milling}), \\ SLE &= \min_{t,j} (r_{y,j}(t)) + \frac{D}{2} \quad (\text{down-milling}). \end{aligned} \tag{23}$$

The SLE depends on various cutting parameters. It is linearly proportional to the feed per tooth f_Z , and in case of straight-edged-tool, it is linearly proportional to the axial depth of cut a_p in case of linear force model. The spindle speed n has a strong nonlinear influence since the natural frequencies of the system could be excited by the Fourier harmonics of the cutting force, which can lead to large resonant vibrations and large SLE values at certain resonant spindle speeds [37]. The SLE is also a nonlinear function of the radial depth of cut, too, as seen in (20). This influence has a key role in the following analysis; therefore, this function is denoted by $s = f_{SLE}(a)$, where $s = SLE/D$ denotes the dimensionless surface location error. This nonlinear function demonstrated in Fig. 3 near the first resonant spindle speed for up-milling (the parameters detailed in Sect. 5).

Note that since the function f_{SLE} is interpreted in the range of $a \in [0, 1]$, where there is no milling for $a = 0$ and full immersion for $a = 1$. We extend the validity range of the function as follows

$$f_{SLE}(a) = \begin{cases} f_{SLE}(0) & \text{if } a < 0, \\ f_{SLE}(a) & \text{if } 0 \leq a \leq 1, \\ f_{SLE}(1) & \text{if } a > 1. \end{cases} \tag{24}$$

This mathematical extension is valid in an engineering point of view, if a is larger than 1, it represents a situation when the tool is completely in the material and if a is less than 0, it represents a case, when the tool does not touch the surface and there is no machining at all.

Note that in this calculation method, first, we define the radial immersion, then we compute the resulting

cutting force and the corresponding vibration, which finally leads to an SLE value [10–12]. In this way, we do not take into account that the SLE can affect its radial depth of cut itself. To describe this phenomenon, we introduce the implicit model, which closes this computational loop in the next section.

4 Implicit model of cumulative surface location error

The dimensionless SLE for the i^{th} consecutive immersion s_i can be calculated by a map as $s_i = f_{\text{SLE}}(a_i)$, where the current dimensionless radial depth of cut a_i is composed by the pre-set radial depth of cut a_0 , the actual error s_i and the previously resulted one s_{i-1} in the form as

$$a_i = a_0 + s_{i-1} - s_i, \tag{25}$$

as shown in Fig. 4a, consequently, the enter and exit angles in (20) can change in each step. Note that there is an analogy between this model and the surface regenerative effect [5], where the actual chip thickness depends on the feed, the present and the delayed positions of the tool. It can be modeled by delay differential equations, while the evaluation of the *SLE* is based on stationary solution. Thus, it can be described as a difference equation realized by the following implicit map

$$s_{i+1} = f_{\text{SLE}}(a_0 + s_i - s_{i+1}), \tag{26}$$

where $f_{\text{SLE}} \in \mathbb{R} \rightarrow \mathbb{R}$ with the state variable s and it is assumed to be smooth. This implicit map can be presented in the same form as the governing equation (1) by considering the following form $f(s_i, s_{i+1}; a_0) = f_{\text{SLE}}(a_0 + s_i - s_{i+1})$. For the special pattern of derivatives, which will be needed for the linear and nonlinear investigations, see detailed derivation in Appendix B.

The implicit map (26) determines how an *SLE* develops into another *SLE* over immersion-by-immersion. The series of the *SLEs* may converge to a fixed point, which is called cumulative surface location error ($\text{CSLE} = \lim_{i \rightarrow \infty} SLE_i$). In other words, fixed point is a state that dynamics maps to itself $s_i = s_{i+1} \equiv s^*$, that is, in the special implicit map in (26), the fixed point can be determined simply by

$$s^* = f_{\text{SLE}}(a_0). \tag{27}$$

It means that every point of the function f_{SLE} is also a fixed point, but still, the surface errors do not always

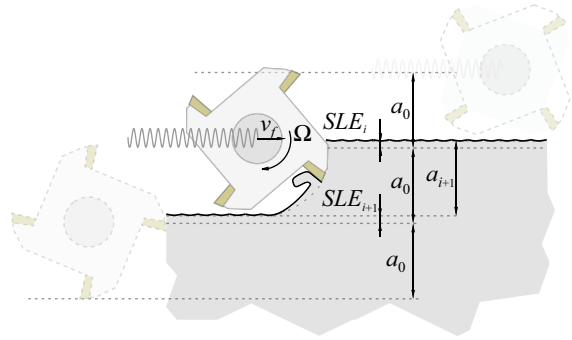


Fig. 4 Schematic model of the surface evaluation in successive immersions

converge here immersion-by-immersion, because it depends on the stability of the fixed point and also on the global dynamics.

4.1 Linear stability analysis

In this section, we analyze the local dynamics in the vicinity of the fixed point. The corresponding characteristic multiplier can be calculated using (9), which simplifies to

$$\mu = \frac{f'_{\text{SLE}}(a_0)}{1 + f'_{\text{SLE}}(a_0)}. \tag{28}$$

As it is shown in (28), μ can be expressed as a hyperbolic function of the derivatives of the $f_{\text{SLE}}(a_0)$ at the fixed point. By investigating (28), one can show that the system loses stability via flip bifurcation $\mu = -1$ (period-2 solutions around the fixed) at a critical pre-set radial depth of cut $a_{0,\text{cr}}$ where

$$f'_{\text{SLE}}(a_{0,\text{cr}}) = -0.5. \tag{29}$$

Note that usual fold (or saddle-node) bifurcation cannot occur in this system since it is not possible that μ reaches 1.

4.2 Nonlinear investigation

In the followings, we derive the required formulas for bifurcation analysis. The root tendencies at the critical point $a_{0,\text{cr}}$ can be calculated according to (14) and using that in case of flip bifurcation (29) holds, which simplifies (14) to

$$\gamma_{\text{cr}} = 4f''_{\text{SLE}}(a_{0,\text{cr}}). \tag{30}$$

Table 1 Technological parameters

Number of edges	Z	3
Tool diameter	D	8 mm
Tool overhang	L	45 mm
Axial depth of cut	a_p	6 mm
Feed per tooth	f_z	0.15 mm
Tangential force coefficient	K_t	$644 \times 10^6 \text{ N/m}^2$
Radial force coefficient	K_r	$237 \times 10^6 \text{ N/m}^2$

The leading coefficients can be calculated for the implicit CSLE model by the formula in (15) considering the special patterns in the derivatives presented in Appendix B

$$\delta_{cr} = -\frac{8}{3} f''_{SLE}(a_{0,cr}). \tag{31}$$

Finally, the approximated oscillations of the period-2 solution in the vicinity of the fixed point based on (13) can be given by

$$u_i = s_i - s^* = \sqrt{-\frac{3 f''_{SLE}(a_{0,cr})}{2 f'''_{SLE}(a_{0,cr})}} (a_0 - a_{0,cr}) (-1)^i. \tag{32}$$

Note that the analysis based on normal form calculation is valid only in the vicinity of the bifurcation point and can catch neither the trend of the period-2 solution farther from the critical point nor the presence of fold bifurcation of period-2 solutions.

5 Case study: cumulative surface error in milling

In this section, we demonstrate numerical bifurcation analysis of the implicit scalar system provided by the evolution of surface errors in case of milling operations. In the conducted case study, all the computations were performed for the parameters presented in Table 1, while the measured tool-tip FRF of a long peripheral milling tool was used, which is shown in Fig. 5.

Figure 6 shows the surface location errors with gray colormap in the plane of the spindle speed n and the dimensionless radial depth of cut a . Here, down-milling and up-milling are represented above each other, as $a = 0$ represents no machining for both cases. It is well-known that large resonant stationary vibrations can occur if one of the natural frequencies is excited by one of the Fourier harmonics of the cutting force.

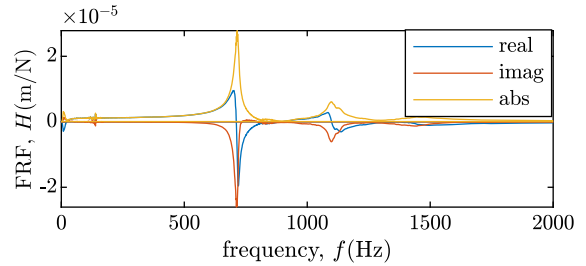


Fig. 5 Measured direct tool-tip's FRF (receptance) in the y direction for the tool described in Table 1 [17]

As a result, considerable SLE is generated at resonant spindle speeds (e.g., $n \approx 14.2, 7.1, 3.55$ krpm).

According to (27), these errors (SLE) are also the fixed points of the implicit model of the surface evolution process (CSLE = Ds^*). The stability properties can be determined with further computation steps, as it is presented in Sect. 2 to ensure that surface error remains in the vicinity of the predicted one after several consecutive immersions.

It is important to note that large surface errors (around 1 in the dimensionless error) are not realistic. In that case, this model is likely to be inadequately, because the corresponding large amplitude resonant vibration can cause the cutting edges to exit the material on a cut-by-cut basis and can influence the enter and exit angles. Furthermore, the circular approximation of the tool path is not valid anymore and some other linear approximations during the modeling lose their validity and nonlinear investigation would be needed [38, 39]. In practice, significant SLE value ($s \gtrsim 0.2$) should be avoided, this the precise calculation this large amplitude vibration is out of scope of this paper.

5.1 Linear investigation

The linear stability limit of the fixed point is calculated by the formula in (29). It can be directly computed in the plane of technological parameters by computing a contour line over a dense grid or by using the so-called multi-dimensional bisection method (MDBM) [40], which is a more efficient algorithm. Note that here we use numeric derivation to calculate f'_{SLE} in (29). These curves correspond to flip bifurcation.

Boundaries of the linearly unstable parameter domains are visualized with green/red curves in Fig. 6. Selecting technological parameters from these domains,

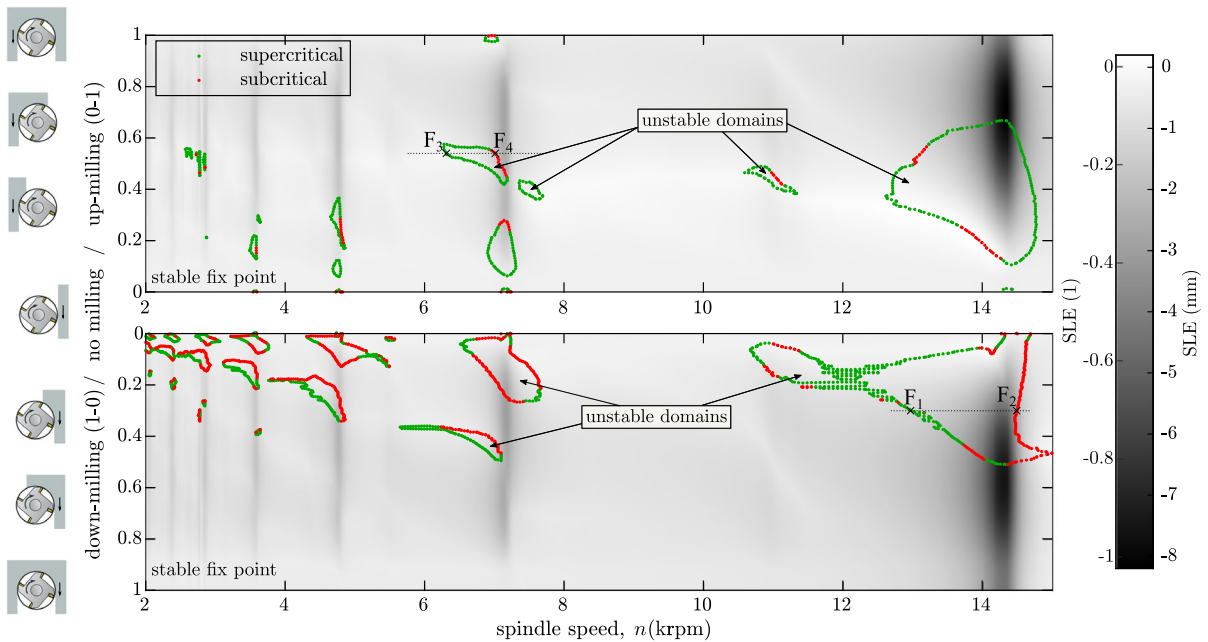


Fig. 6 Stability charts of the fixed point of the *CSLE* model; Red contour represents the location of subcritical flip bifurcation while green refers to the supercritical ones, gray scale shows the magnitude of the calculated fixed points. Note, however, the

milling model at $a = 0$ and $a = 1$ provides the same SLE, the gradient are different leading to different *CSLE* stability behavior. (color figure online)

the final surface error cannot be predicted at the end of the roughing operation due to the fact that the SLE diverges from the fixed point at each immersion. Thus, the oversize of the workpiece will be uncertain before the finishing operation, therefore the corresponding technological parameters may be unfavourable during the process design. Note that chatter vibrations due to classical regenerative effect may occur along with the *CSLE* stability problem [17]; however, it is out of the scope of the current work.

Note that chatter and *CSLE* stability are not mutually exclusive; however, typically one can be found where the other is not. Unfortunately, the *CSLE* stability problem is more typical at favorable pockets of the stability lobes of classical regenerative vibrations (chatter) near the resonant spindle speeds.

5.2 Nonlinear investigation

The bifurcation analysis is carried out based on Sect. 4.2. The criticality of the flip bifurcation is investigated based on the sign of the normal form coefficient

δ_{cr} in (31). In case of supercritical/subcritical bifurcation (which are marked by green and red dots in Fig. 6, respectively), a branch of stable/unstable periodic-2 solution emerges from the flip points. Note that where green and red curves are met, the bifurcation is non-generic since the normal form coefficient is zero. To get a clear view of the global dynamics, Fig. 7 present the bifurcation diagrams along horizontal cross sections at $a = 0.3$ for down-milling and $a = 0.54$ for up-milling (see dotted lines in Fig. 6). Here, the approximated amplitude of the surface error oscillations around the fixed point are plotted with black dashed curves as a function of the bifurcation parameter n (spindle speed). Note that for the fixed point, this amplitude is zero corresponding to the horizontal axis. For down-milling, as shown in Fig. 7a the fixed point is unstable for spindle speeds $n \in [13, 14.5]$ krpm, while for up-milling operation (see Fig. 7b), it is unstable between $n \in [6.3, 7]$ krpm. The flip bifurcations, denoted in both panels by F_1, F_3 and F_2, F_4 , are supercritical and subcritical, respectively.

From the engineering point of view, the subcritical case is the more dangerous, since it causes an unstable

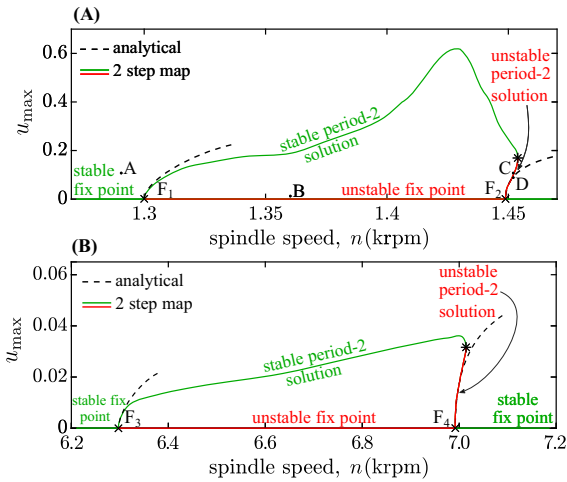


Fig. 7 Bifurcation diagrams for down-milling operation **a** near the first resonant spindle speed around $n \approx 14$ krpm at $a = 0.3$ radial depth of cut and for up-milling **b** near the second resonant spindle speed at $a = 0.54$ radial depth of cut (see dotted lines in Fig. 6). Stable and unstable solutions are presented as green and red curves, respectively. Black dashed curves are the results of analytical normal form calculations while colored curves are obtained by the two-step map. The supercritical (F_1, F_3) and subcritical (F_2, F_4) flip bifurcation points are marked by black crosses while fold bifurcations of the period-2 solutions are denoted by black stars. (color figure online)

period-2 solution around the linearly stable fixed point. It also indicates the presence of a stable period-2 solution by folding back this unstable one, which creates a bistable parameter region (see a similar phenomenon in [41]). Here, the final surface location error can converge either to a stable fixed point or to a stable period-2 solution depending on initial conditions. Consequently, this bistable parameter domain increases the unfavorable parameter range even further.

5.3 Two-step mapping and verification

The verification of the analytical results of the emerging branches could be performed by means of long numerical iterations for different bifurcation parameter values. This is computationally inefficient and leads to errors close to bifurcation points due to the very slow converging solutions ($|\mu| \approx 1$). However, a computationally more efficient technique can be used based on the direct computation of all the period-2 solutions along the bifurcation parameter. Two-step mapping of (26) must be considered by substituted successively into itself

$$\begin{bmatrix} s_{i+1} \\ s_{i+2} \end{bmatrix} = \begin{bmatrix} f_{SLE}(a_0 + s_i - s_{i+1}) \\ f_{SLE}(a_0 + s_{i+1} - s_{i+2}) \end{bmatrix}. \tag{33}$$

In case of period-2 solutions, all the even and odd values are the same $s_0 = s_2 = \dots =: s_0^*$ and $s_1 = s_3 = \dots =: s_1^*$. Considering these properties in (33), the period-2 solutions $s_{0,1}^*$ can be calculated by means of solving the following equations

$$\begin{bmatrix} s_0^* \\ s_1^* \end{bmatrix} - \begin{bmatrix} f_{SLE}(a_0 + s_1^* - s_0^*) \\ f_{SLE}(a_0 + s_0^* - s_1^*) \end{bmatrix} = \begin{bmatrix} 0 \\ 0 \end{bmatrix}. \tag{34}$$

One can directly compute these solutions within a selected domain of spindle speed by means of the MDBM, which can find the solution curves for three variables (n, s_0^*, s_1^*) for two implicit nonlinear equations. The maximum amplitude of u of the calculated period-2 solutions are plotted with continuous curves in Fig. 7. As expected, the approximated analytically calculated bifurcation curves (black dashed curves) well follow the trend of the numerical solution near the fixed point.

The stability of the period-2 solutions provided by the two-step map can be analyzed by the implicit function derivation theorem presented in [29]. In Fig. 7, stable and unstable period-2 solutions are colored with green and red, respectively. Note that in contrast to the fixed point where only flip bifurcation occurs, here, fold type stability loss can also happen. This fold point (denoted by black stars) takes place where stable and unstable period-2 solutions merge.

Note that period- p solution can be constructed in a similar way which is briefly presented in Appendix C, for which the linear stability behavior can be determined based on [42].

5.4 Numeric iteration

In order to illustrate different kind of behavior during the evolution process of the surface error, four points were selected in Fig. 7a and successive implicit iteration of (26) based on [43,44] were performed. These iterations are not straightforward because multiple solution can exist for implicit equations (1) or (26), thus the uniqueness of the solution is not guaranteed. We bypassed this problem in the implementation of the numerical computation: we calculated the new solutions by a Newton–Raphson method starting from the previous solution which provides only a single solution. This issue could be solved with dynamic time-domain

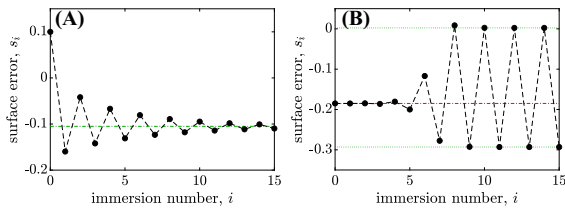


Fig. 8 The evolution of the dimensionless surface location errors immersion-by-immersion in case of linearly stable and unstable fixed point for parameter points A ($n = 12.8$ krpm) and B ($n = 13.6$ krpm) in Fig. 7a

simulation which takes into account complex interaction between tool-workpiece engagement during forced vibration [38,39], but it would require excessive computational resources and loses the advantages of the relatively simple solution offered by the implicit model.

The surface errors are plotted immersion-by-immersion in Figs. 8 and 9. A globally stable case is illustrated in Fig. 8a, where after an initial oscillation, the surface location error converges to the stable fixed point (green dash-dotted line). Panel b represents the case for a linearly unstable fixed point, where alternating surface errors emerge due to the small initial perturbation of the fixed point, which tends to the period-2 solution (green dotted lines).

The behavior in case of bistable parameter region is illustrated in Fig. 9. Here, we use the same technological parameters and start the iteration from two different initial conditions, which highlights the role of the unstable period-2 solution (red dotted lines). In our case study, if we select an initial value between the unstable period-2 solution (s_0^{*U}, s_1^{*U}), the surface error converges to the stable fixed point (panel a), otherwise, it goes to the stable period-2 solution (s_0^{*S}, s_1^{*S}) (panel b). In other words, the unstable period-2 solution determines a threshold that separates the attraction zone of the stable solutions.

From the viewpoint of the CSLE stability problem, during the parameter design of roughing operation, the globally stable fixed point (point A) can be acceptable because in all other cases, the oversize of the workpiece may not be precisely predicted before the finishing process.

6 Conclusion

In this study, we introduce an approach to analyze the bifurcations of implicit scalar maps. The presented

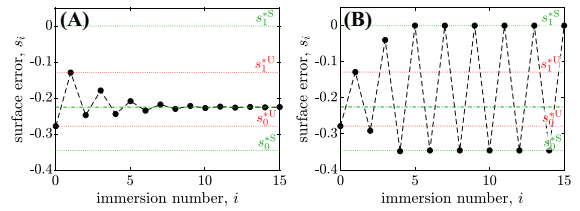


Fig. 9 The evolution of the dimensionless surface location errors immersion-by-immersion in case of bistable parameter point at $n = 14.52$ krpm and $a = 0.3$ during down-milling for different initial conditions. The initial conditions for point a is $s_0 = -0.2783$ while for point b is $s_0 = -0.2784$. See the location C and D in Fig. 7a

method uses the Implicit Function Theorem and its differentiation form. Analytical formulae for normal form coefficients are derived, from which approximated amplitude and stability of the arising solutions and criticality of the bifurcation point can be determined.

The derived theory for implicit maps was applied in an engineering problem. The evolution of surface errors during roughing operations was investigated. The essence of the proposed method is the introduction of the novel implicit map, which takes into account not only the effects of the past but also the effects of the current state, while it describes how one error develops into another. The stability analysis of this problem shows that the final surface location error cannot be predicted at the end of the roughing process, which can affect the finishing operation. In addition, we have shown that stability loss can not only occur in resonant spindle speeds (where a large surface location error occurs), but it can also happen where the surface error itself is small, but has a large derivative along with the radial depth of cut. Also, we proved that only flip-type bifurcation could occur for the SLE model, which may lead to alternating final surface errors. With the proposed method, the traditional stability chart relating to the regenerative effect can be extended, from which chatter-free and CSLE stable technological parameters can be selected in order to support the technological design.

During the nonlinear investigations of the special milling case, we utilized further simplifications to determine the coefficients of the normal form. It has shown that bistable parameter ranges can also occur due to the presence of subcritical flip bifurcation. From the engineering point of view, it must also be avoided since

these domains further increase the range of the uncertain SLE prediction. These analyses may open ways for efficient cutting parameter optimization strategies crossing the border toward reliable and optimal cutting. Our further goals are to perform measurements for the surface error problems to validate and support the theoretical results.

Although, the proposed bifurcation analysis of nonlinear implicit maps is applied only on milling example, this could be used generally in any application field. To support general usage, it is still left for future work to extend the normal form computation for systems with higher dimensions.

Acknowledgements The research reported in this paper has been supported by the National Research, Development and Innovation Fund (TKP2020 NC, Grant No. BME-NCS and TKP2021, Project no. BME-NVA-02) under the auspices of the Ministry for Innovation and Technology and by the Hungarian National Research, Development and Innovation Office (Grant no. NKFI FK-124462 and FK-138500).

Funding Open access funding provided by Budapest University of Technology and Economics. NRDIFund: TKP2020 NC, Grant No. BME-NCS; Hungarian Scientific Research Fund, FK-124462; Hungarian Scientific Research Fund (HU); Adam K. Kiss, NRDIFund: TKP2020 NC, Grant No. BME-NVA; Nemzeti Kutatási, Fejlesztési és Innovációs Alap.

Data availability The authors declare that data supporting the findings of this study are available within the article.

Declarations

Conflict of interest The authors declare that they have no conflict of interest.

Open Access This article is licensed under a Creative Commons Attribution 4.0 International License, which permits use, sharing, adaptation, distribution and reproduction in any medium or format, as long as you give appropriate credit to the original author(s) and the source, provide a link to the Creative Commons licence, and indicate if changes were made. The images or other third party material in this article are included in the article’s Creative Commons licence, unless indicated otherwise in a credit line to the material. If material is not included in the article’s Creative Commons licence and your intended use is not permitted by statutory regulation or exceeds the permitted use, you will need to obtain permission directly from the copyright holder. To view a copy of this licence, visit <http://creativecommons.org/licenses/by/4.0/>.

Appendix A

For the bifurcation analysis of the implicit system in (1), the second- $g''(x^*)$ and third-order $g'''(x^*)$ terms in the approximation of the explicit map (3) are also needed. These can be similarly defined as presented for $g'(x^*)$ in Sect. 2.2. The second-order total differentiation of (2) with the substitution $x_{i+1} = g(x_i)$ leads to

$$\begin{aligned} & \frac{d^2}{dx_i^2} F(x_i, g(x_i)) = \\ & \frac{\partial^2 F}{\partial x_i^2} + 2 \frac{\partial^2 F}{\partial x_i \partial g(x_i)} g'(x^*) + \frac{\partial F}{\partial g(x_i)} g''(x^*) = 0. \end{aligned} \tag{35}$$

The second-order partial derivatives simplify to $\frac{\partial^2 F}{\partial x_i^2} = \frac{\partial^2 f}{\partial x_i^2}$ and $\frac{\partial^2 F}{\partial x_i \partial g(x_i)} = \frac{\partial^2 F}{\partial x_i \partial x_{i+1}} = \frac{\partial^2 f}{\partial x_i \partial x_{i+1}}$. Finally, substituting (7) and rearranging the terms results in

$$g''(x^*) = - \frac{(f_b - 1)(f_{aa} - 2f_a f_{ab} - f_{aa} f_b) - f_a^2 f_{bb}}{(f_b - 1)^3} \Big|_{x^*}. \tag{36}$$

Here, we use the same short notation as presented after 15.

Considering the critical parameter in (9), (36) can be simplified for flip bifurcation ($\mu = -1$):

$$g''(x^*) = - \frac{f_{aa} - 2f_{ab} + f_{bb}}{f_a} \Big|_{x^*} \tag{37}$$

and for the fold bifurcation ($\mu = 1$):

$$g''(x^*) = \frac{f_{aa} + 2f_{ab} + f_{bb}}{f_a} \Big|_{x^*}. \tag{38}$$

The third-order $g'''(x^*)$ term, which is necessary for the normal form calculation of the flip bifurcation, can be calculated by computing the third-order total differentiation of (2):

$$\frac{d^3}{dx_i^3} F(x_i, g(x_i)) = 0, \tag{39}$$

from which, one can express $g'''(x^*)$ considering $\mu = -1$ as

$$g'''(x^*) = \frac{3(f_{ab} - f_{bb})(f_{aa} - 2f_{ab} + f_{bb}) - f_a^2 f_{bb}}{f_a(f_{aaa} - 3f_{aab} + 3f_{abb} + f_{bbb})} \Big|_{x^*}. \tag{40}$$

Appendix B

In case of the milling example, the following relations for the partial derivatives of the function $f_{SLE}(a_0 + s_i - s_{i+1})$ hold

$$f'_{SLE}(a_0) := \frac{\partial f_{SLE}}{\partial a_0} \Big|_{a_0} = \frac{\partial f_{SLE}}{\partial s_i} \Big|_{a_0} = - \frac{\partial f_{SLE}}{\partial s_{i+1}} \Big|_{a_0} \quad (41)$$

$$f''_{SLE}(a_0) := \frac{\partial^2 f_{SLE}}{\partial a_0^2} \Big|_{a_0} = \frac{\partial^2 f_{SLE}}{\partial s_i^2} \Big|_{a_0} = \frac{\partial^2 f_{SLE}}{\partial s_{i+1}^2} \Big|_{a_0} = - \frac{\partial^2 f_{SLE}}{\partial s_i \partial s_{i+1}} \Big|_{a_0} = \frac{\partial^2 f_{SLE}}{\partial s_i \partial a_0} \Big|_{a_0} = - \frac{\partial^2 f_{SLE}}{\partial s_{i+1} \partial a_0} \Big|_{a_0} \quad (42)$$

$$f'''_{SLE}(a_0) := \frac{\partial^3 f_{SLE}}{\partial a_0^3} \Big|_{a_0} = \frac{\partial^3 f_{SLE}}{\partial s_i^3} \Big|_{a_0} = - \frac{\partial^3 f_{SLE}}{\partial s_{i+1}^3} \Big|_{a_0} = - \frac{\partial^3 f_{SLE}}{\partial s_i^2 \partial s_{i+1}} \Big|_{a_0} = \frac{\partial^3 f_{SLE}}{\partial s_i \partial s_{i+1}^2} \Big|_{a_0} \quad (43)$$

which simplify the formulae of the root tendency in (14) and the leading coefficient in (15) to (30) and (31), respectively.

Appendix C

Here, we briefly discuss the calculation steps for determining period- p solution and its stability property. First, p consecutive map of (1) are considered and represented as a multi-variable mapping: the p -step-mapping in the following way

$$\underbrace{\begin{bmatrix} s_{i+1} \\ s_{i+2} \\ \vdots \\ s_{i+p} \end{bmatrix}}_{s_{i+1}} = \underbrace{\begin{bmatrix} f(s_i, s_{i+1}) \\ f(s_{i+1}, s_{i+2}) \\ \vdots \\ f(s_{i+p-1}, s_{i+p}) \end{bmatrix}}_{\mathbf{f}(s_i, s_{i+1})} \quad (44)$$

where $s_i \in \mathbb{R}^p$ collects the state variables and $\mathbf{f} : \mathbb{R}^p \times \mathbb{R}^p \rightarrow \mathbb{R}^p$ is vector valued. The p -step-mapping problem can be reformulated as

$$\mathbf{F}(s_i, s_{i+1}) := \mathbf{f}(s_i, s_{i+1}) - s_{i+1} = \mathbf{0}, \quad (45)$$

where \mathbf{F} has the same properties as \mathbf{f} . According to the periodicity condition, every p th values are the same, that reads $s_i = s_{i+kp} =: s_j^*$, where $k = 1, 2, \dots$ and $j = i \bmod p$. Considering these properties, the period- p solutions be denoted by $s_0^* = \text{col}_{j=0}^{p-1} s_j^*$. Note that $s_1^* = \mathbf{C}s_0^*$, where \mathbf{C} is the circular shift matrix. The

periodic solution can be calculated based on the nonlinear equations $\mathbf{F}(s_0^*, \mathbf{C}s_0^*) = \mathbf{0}$ constructed as follows:

$$\begin{bmatrix} f(s_0^*, s_1^*) \\ f(s_1^*, s_2^*) \\ \vdots \\ f(s_{p-2}^*, s_{p-1}^*) \\ f(s_{p-1}^*, s_0^*) \end{bmatrix} - \begin{bmatrix} s_1^* \\ s_2^* \\ \vdots \\ s_{p-1}^* \\ s_0^* \end{bmatrix} = \begin{bmatrix} 0 \\ 0 \\ \vdots \\ 0 \\ 0 \end{bmatrix}. \quad (46)$$

References

- Munoa, J., Beudaert, X., Dombovari, Z., Altintas, Y., Budak, E., Brecher, C., Stepan, G.: Chatter suppression techniques in metal cutting, vol. 65. In: 66th General Assembly of the International-Academy-for-Production-Engineering, Guimaraes (Portugal), 21 Aug 2016–27 Aug 2016, CIRP, pp. 785–808 (2016)
- Altintas, Y.: Manufacturing Automation—Metal Cutting Mechanics, Machine Tool Vibrations and CNC Design, 2nd edn. Cambridge University Press, Cambridge (2012)
- Tlusty, J.: Effect of end milling deflections on accuracy. In: Handbook of High-speed Machining Technology, pp. 140–153 (1985)
- Tlusty, J., Spacek, L.: Self-excited vibrations on machine tools, Nakl. CSAV, Prague, in Czech (1954)
- Tobias, S.: Machine-Tool Vibration. Blackie, Glasgow (1965)
- Stepan, G.: Retarded Dynamical Systems. Longman, Harlow (1989)
- Altintas, Y., Budak, E.: Analytical prediction of stability lobes in milling. CIRP Ann. Manuf. Techn. **44**, 357–362 (1995)
- Mann, B.P., Young, K.A., Schmitz, T.L., Dilley, D.N.: Simultaneous stability and surface location error predictions in milling. J. Manuf. Sci. Eng. **127**(3), 446–453 (2004)
- Wang, D., Wang, X., Liu, Z., Gao, P., Ji, Y., Löser, M., Ihlenfeldt, S.: Surface location error prediction and stability analysis of micro-milling with variation of tool overhang length. Int. J. Adv. Manuf. Technol. **99**(1–4), 919–936 (2018)
- Kline, W., DeVor, R., Lindberg, J.: The prediction of cutting forces in end milling with application to cornering cuts. Int. J. Mach. Tool Des. Res. **22**(1), 7–22 (1982)
- Schmitz, T.L., Ziegert, J.C., Canning, J.S., Zapata, R.: Case study: a comparison of error sources in high-speed milling. Precis. Eng. **32**(2), 126–133 (2008)
- Altintas, Y., Montgomery, D., Budak, E.: Dynamic peripheral milling of flexible structures. J. Eng. Indust. **114**(2), 137–145 (1992)
- Inspurger, T., Gradisek, J., Kalveram, M., Stepan, G., Winert, K., Govekar, E.: Machine tool chatter and surface location error in milling processes. J. Manuf. Sci. Eng. **128**, 913–920 (2006)
- Bachrathy, D., Munoa, J., Stepan, G.: Experimental validation of appropriate axial immersions for helical mills. Int. J. Adv. Manuf. Technol. 1–8 (2015)
- Kiss, A.: Cumulative surface location error for cutting processes, Master’s thesis, Budapest University of Technol-

- ogy and Economics, Department of Applied Mechanics, Budapest, Hungary (2014)
16. Kiss, A., Bachrathy, D.: Explicit model of cumulative surface location error for milling processes. In: 12th Hungarian Conference on Theoretical and Applied Mechanics HCTAM. University of Miskolc, Department of Mechanical Engineering and Informatics, Institute of Applied Mechanics (2015)
 17. Kiss, A., Bachrathy, D., Stepan, G.: Cumulative surface location error for milling processes based on tool-tip frequency response function. *PROCEDIA CIRP* **46**, 323–326 (2016)
 18. Wang, D., Löser, M., Luo, Y., Ihlenfeldt, S., Wang, X., Liu, Z.: Prediction of cumulative surface location error at the contact zone of in-process workpiece and milling tool. *Int. J. Mech. Sci.* 105543 (2020)
 19. Kiss, A.K., Bachrathy, D.: Experimental validation of cumulative surface location error for turning processes. *Acta Polytechnica CTU Proc.* **3**, 25–29 (2016)
 20. Guckenheimer, J.: On the bifurcation of maps of the interval. *Invent. Math.* **39**(2), 165–178 (1977)
 21. Whitley, D.: Discrete dynamical systems in dimensions one and two. *Bull. Lond. Math. Soc.* **15**(3), 177–217 (1983)
 22. Arnold, V.I.: *Geometrical Methods in the Theory of Ordinary Differential Equations*, vol. 250. Springer Science & Business Media (2012)
 23. Zhao, X., Orosz, G.: Nonlinear day-to-day traffic dynamics with driver experience delay: modeling, stability and bifurcation analysis. *Physica D* **275**, 54–66 (2014)
 24. Molnár, T.G., Dombóvári, Z., Insperger, T., Stépán, G.: Bifurcation analysis of nonlinear time-periodic time-delay systems via semidiscretization. *Int. J. Numer. Meth. Eng.* **115**(1), 57–74 (2018)
 25. Habib, G., Rega, G., Stepan, G.: Nonlinear bifurcation analysis of a single-dof model of a robotic arm subject to digital position control. *J. Comput. Nonlinear Dyn.* **8**(1)
 26. Kuznetsov, Y.A.: *Elements of Applied Bifurcation Theory*, vol. 112. Springer Science & Business Media (2013)
 27. Guckenheimer, J., Holmes, P.: *Nonlinear Oscillations, Dynamical Systems, and Bifurcations of Vector Fields*. Springer, New York (1983)
 28. Butcher, J.C., Goodwin, N.: *Numerical Methods for Ordinary Differential Equations*, vol. 2. Wiley Online Library (2008)
 29. Di Bernardo, M., Vasca, F.: Discrete-time maps for the analysis of bifurcations and chaos in dc/dc converters. *IEEE Tran. Circ. Syst. I Fund. Theory Appl.* **47**(2), 130–143 (2000)
 30. Acary, V., Brogliato, B., Orlov, Y.V.: Chattering-free digital sliding-mode control with state observer and disturbance rejection. *IEEE Trans. Autom. Control* **57**(5), 1087–1101 (2011)
 31. Luo, A.C.: *Discretization and Implicit Mapping Dynamics*. Springer (2015)
 32. Orosz, G., Zhao, X.: Normal form calculations for day-to-day traffic dynamics. In: Ecker, H., Steindl, A., Jakubek, S., (eds.) ENOC 2014–Proceedings of 8th European Nonlinear Dynamics Conference. Institute of Mechanics and Mechatronics, Vienna University of Technology, Vienna, Austria (2014)
 33. Szalai, R., Stepan, G.: Unstable period doubling vibrations in highly interrupted cutting processes. In: *Proceedings of the 5th International Conference on Vibration Engineering* (2002)
 34. Dombóvári, Z., Iglesias, A., Zatarain, M., Insperger, T.: Prediction of multiple dominant chatter frequencies in milling processes. *Int. J. Mach. Tool. Manuf.* **51**, 457–464 (2011)
 35. Kienzle, O.: Spezifische schnittkräfte bei der metallbearbeitung. *Werkstattstechnik und Maschinenbau* **47**, 224–225 (1957)
 36. Budak, E., Altintas, Y., Armarego, E.J.A.: Prediction of milling force coefficients from orthogonal cutting data. *J. Manuf. Sci. Eng.* **118**(2), 216–224 (1996)
 37. Schmitz, T.L., Mann, B.P.: Closed-form solutions for surface location error in milling. *Int. J. Mach. Tools Manuf.* **46**(12), 1369–1377 (2006)
 38. Munoa, J., Dombóvári, Z., Mancisidor, I., Yang, Y., Zatarain, M.: Interaction between multiple modes in milling processes. *Mach. Sci. Technol.* **17**, 165–180 (2013)
 39. Totis, G., Insperger, T., Sortino, M., Stepan, G.: Symmetry breaking in milling dynamics. *Int. J. Mach. Tools Manuf.* **139**, 37–59 (2019). <https://doi.org/10.1016/j.ijmachtools.2019.01.002>
 40. Bachrathy, D., Stepan, G.: Bisection method in higher dimensions and the efficiency number. *Period. Polytech. Mech. Eng.* **56**(2), 81–86 (2012)
 41. Dombóvári, Z., Iglesias, A., Molnar, T.G., Habib, G., Munoa, J., Kuske, R., Stepan, G.: Experimental observations on unsafe zones in milling processes. *Philos. Trans. Roy. Soc. A* **377**(2153), 20180125 (2019)
 42. Luo, A.C.: Periodic flows to chaos based on discrete implicit mappings of continuous nonlinear systems. *Int. J. Bifurc. Chaos* **25**(03), 1550044 (2015)
 43. Xu, H.-K., Ori, R.G.: An implicit iteration process for non-expansive mappings. *Numer. Funct. Anal. Optim.* **22**(5–6), 767–773 (2001)
 44. Huang, N.-J.: Mann and ishikawa type perturbed iterative algorithms for generalized nonlinear implicit quasi-variational inclusions. *Comput. Math. Appl.* **35**(10), 1–7 (1998)

Publisher's Note Springer Nature remains neutral with regard to jurisdictional claims in published maps and institutional affiliations.